JOURNAL OF GEOPHYSICAL RESEARCH, VOL. 102, NO. E11, PAGES 25,593–25,603, NOVEMBER 25, 1997

Determination of Martian meteorite lithologies and mineralogies using vibrational spectroscopy

Victoria E. Hamilton and Philip R. Christensen
Department of Geology, Arizona State University, Tempe

Harry Y. McSween Jr.
Department of Geological Sciences, University of Tennessee, Knoxville

Abstract. We have acquired thermal infrared emission spectra of four Martian meteorite samples, ALH77005, Nakhla, Zagami, and EET79001, representing three major lithologies (lherzolite, clinopyroxenite, and basalt). The spectra of these meteorites are significantly different from each other, and we can distinguish the three lithologies easily on the basis of their spectral morphologies. Using a linear deconvolution model, the modal mineralogies of ALH77005, Nakhla, and Zagami were derived from their spectra to within 2–19% of the modes derived by optical methods. For Zagami and EET79001, the correct mineral types were identified as present using the linear method, although an exact spectral match using available end-member spectra was not obtained, probably due to the lack of a pigeonite end-member spectrum or shock effects in the meteorites. The meteorite spectra we have acquired will be used for comparison with data to be returned by the thermal emission spectrometer (TES) on the Mars Global Surveyor orbiter and would also be useful for comparing to future rover- or lander-based thermal IR spectra. Based on our results, comparisons of mineral end-member and meteorite spectra with TES spectra of coarse regolith and rocky regions should aid identification and mapping of Martian surface lithologies and unit mineralogy.

1. Introduction

The SNC (shergottites, nakhlites, and Chassigny) meteorites are distinctive achondrites with igneous compositions ranging from basaltic to ultramafic (summarized by *McSween* [1985]). Based on geochemical dating techniques, most of these samples are postulated to have crystallization ages of 1.3 Gyr or younger [*Shih et al.*, 1982; *Nyquist et al.*, 1984; *Jagoutz and Wänke*, 1985; *Jones*, 1985]. Such young ages require a parent body that was geologically active (and differentiating) late into its history, implying a body of planetary size. Trapped gases in SNCs have unusual relative isotopic abundances and compositions that are unique among meteorites, but are very similar to the Martian atmosphere as measured by Viking [*Bogard et al.*, 1984; *Becker and Pepin*, 1984; *Swindle et al.*, 1984]. These unique characteristics point to Mars as the probable parent body of the SNC meteorites [e.g., *Wood and Ashwal*, 1981; *McSween*, 1984]. There are currently 12 recognized Martian meteorites, and interest in these meteorites has risen to new levels with the suggestion that one of the 12, ALH84001, may contain evidence for primordial life on Mars [*McKay et al.*, 1996].

Two spectroscopic methods, based on the interaction of light with either electronic transitions or the vibrational motions of atoms and molecules, are commonly used to study geologic materials. Electronic spectra exhibit absorptions due to electronic transitions in transition series elements, of which Fe is the most geologically common. Spectral absorptions due to electronic transitions are measured in the visible to near-infrared (VNIR) region of the electromagnetic spectrum (0.35–2.5 μm). Several excellent studies of the surface of Mars have used electronic spectroscopy [*Adams*, 1968; *Singer*, 1980a, b; *Singer and Roush*, 1985; *Erard et al.*, 1990; *Mustard et al.*, 1990, 1993; *Soderblom*, 1992; *Roush et al.*, 1993]. Absorptions in VNIR spectra of the bright and dark regions of Mars, with the exception of bands due to atmospheric CO_2, are all attributed to the presence of Fe^{2+} and Fe^{3+} [*Roush et al.*, 1993], and *McSween* [1994] suggested that near-infrared spectra of dark, presumably rocky regions [*Singer et al.*, 1980b; *Mustard et al.*, 1993] imply that crustal rocks are mineralogically similar to shergottites. Furthermore, *Mustard and Sunshine* [1995] showed correspondence between the electronic spectra of Martian meteorites and the mineralogy of dark regions of Mars. Although the absorptions in electronic spectra can provide useful information about several mineralogical compositions (e.g., pyroxenes and olivines), a significant number of minerals of geological importance are not composed of transition elements. Additionally, electronic spectra are poor indicators of absolute modal mineral abundances in the case of mineral mixtures (synthetic or rock) due to the complicating effects of multiple scattering.

Vibrational spectroscopy is a technique which is sensitive to the unique structure and chemical composition of every mineral. All minerals display a unique spectral signature due to vibrational modes resulting from the stretching and bending vibrations of atoms in the crystal lattices of minerals. Fundamental vibrational absorptions of geologic materials occur in the range from ~3 to 50 μm (thermal infrared), and in some minerals, vibrational overtones and/or combination modes associated with hydroxyls, bound water, carbonate, etc., extend into the visible to near-infrared portion of the spectrum. Vi-

Paper number 97JE01874.
0148-0227/97/97JE-01874$09.00

brational motions occur at specific, quantized frequencies, and when incident electromagnetic energy corresponds to one of these frequencies, the result is the excitation of a specific vibration and an absorption feature in the spectrum. In minerals, bond strength, as well as cation coordination and substitution, affect the vibrational energy of the crystal lattice, resulting in variations in the dominant wavelengths of absorption from mineral to mineral. The number, relative strength, and wavelength positions of absorptions in the spectrum of each mineral are unique. Thus the spectral "signature" of each mineral serves as a means of identifying that mineral. Furthermore, the spectra of a rock's constituent minerals add approximately linearly in the thermal infrared to produce the rock's spectrum because very high absorption coefficients result in few multigrain interactions. Therefore the composition of a rock may be determined by linear deconvolution as explained below.

Previous work with vibrational spectra of Martian meteorites includes that of *Bishop et al.* [1994] and *Salisbury et al.* [1991a]. The *Bishop et al.* [1994] study acquired thermal infrared reflectance spectra of the meteorite ALH84001 from 1300 to 400 cm^{-1} (~7.7–25 μm) and showed that the spectrum of the meteorite resembles the spectrum of its primary consituitent (>90%), orthopyroxene. The work of *Salisbury et al.* [1991a] described midinfrared biconical reflectance spectra of powdered (approximately $\leq$70 μm) meteorite samples, including the shergottites ALH77005 and EET79001, over the wavelength range 4000 to ~740 cm^{-1} (2.5–13.5 μm). At thermal infrared wavelengths the spectra of powdered samples (less than ~65 μm in diameter) display different features than the spectra of larger samples due to scattering at grain boundaries where the grain size is comparable to the wavelength [e.g., *Lyon*, 1964; *Aronson et al.*, 1966; *Hunt and Vincent*, 1968; *Vincent and Hunt*, 1968; *Hunt and Logan*, 1972; *Aronson and Emslie*, 1973; *Salisbury and Eastes*, 1985; *Salisbury and Wald*, 1992; *Moersch and Christensen*, 1995; *Mustard and Hays*, 1997]. To eliminate these effects, we have used bulk meteorite samples and coarse particulate mineral samples with grain sizes significantly larger than the wavelength of energy being studied. Spectra of powdered samples should be useful for modeling particulate surfaces, and bulk sample spectra will provide spectral information for comparison with the coarse (>100 μm) regolith, rocky terrains, and bedrock exposures expected over much of the Martian surface [*Palluconi and Kieffer*, 1981; *Christensen*, 1986]. Additionally, while hemispherical reflectance spectra and emission spectra can be related via Kirchhoff's law ($\varepsilon = 1 - R$) [*Hapke*, 1993], biconical reflectance data are not quantitatively comparable to emission data [*Salisbury and Wald*, 1992].

The thermal emission spectrometer (TES) instrument was launched to Mars on the Mars Global Surveyor in November 1996 for the purposes of mapping the mineralogy and thermal properties of the Martian surface and studying the planet's atmosphere [*Christensen et al.*, 1992]. This instrument will acquire data over the thermal infrared region from ~1600 to 200 cm^{-1} (6–50 μm), where all mineral spectra exhibit unique combinations of absorption features. Laboratory spectra of Martian meteorites will be compared with spectra that will be collected by the TES and may facilitate a search for the source regions of these meteorites.

The primary objective of this paper is to demonstrate that by using the thermal infrared emission technique, we can distinguish the various lithologies of the meteorites and determine their mineralogies, information which should be valuable in the interpretation of spectral data acquired from Martian orbit. We first review the mineralogy of the four Martian meteorites we examined, describe our experimental technique, and discuss the spectral characteristics of the meteorites. We then evaluate the results of a linear deconvolution method for determination of the mineralogy of each sample from its spectrum.

2. Meteorite Samples

We have studied samples of four Martian meteorites: Nakhla, ALH77005, Zagami, and EET79001. These samples were selected to obtain a variety of pyroxene-bearing lithologies. In this section, we will briefly describe the origin and mineralogic characteristics of each meteorite.

Our sample of Nakhla (USNM 426) is a single pyramidal piece weighing 21.3 g and measuring approximately 2.5 cm on each side. Nakhla is an unshocked clinopyroxenite dominated by augite (79 vol %), with olivine (16%) and plagioclase feldspar (4%); augite compositions are $En_{37.9}$ $Fs_{23.0}$ $Wo_{39.1}$, olivine is iron-rich (fayalitic) with a composition of $Fo_{32.0}$, and plagioclase feldspar is intermediate in composition, about $An_{23.0-26.0}$ [*Berkley et al.*, 1980]. Olivine content fluctuates between 5 and 18% in Nakhla specimens (R. C. Friedman, personal communication, 1996); as olivine content decreases, augite content increases [*Friedman et al.*, 1994]. Other phases include K feldspar (1%), titanomagnetite (2%), and various trace oxides and sulfides [*Bunch and Reid*, 1975; *Berkley et al.*, 1980]. Augite grains are approximately 1.0 by 0.3 mm in size, while olivine grains are slightly larger, from 1.0 to 1.6 mm, and interstitial feldspar laths may be up to 0.3 mm long and 0.1 mm wide [*Bunch and Reid*, 1975]. The crystallization age of Nakhla has been estimated at 1.3 Gyr by *Gale et al.* [1975] and *Nakamura et al.* [1982].

ALH77005 is a lherzolitic shergottite [*McSween et al.*, 1979; *Ikeda*, 1994]. Our sample, obtained through the Antarctic Meteorite Collection at Johnson Space Center, consists of two pieces measuring approximately 1.5 × 1.2 × 0.5 and 1.0 × 1.0 × 0.8 cm. This meteorite has a poikilitic texture and is composed of approximately 37% pyroxene, 52% olivine, and 10% maskelynite (shocked plagioclase feldspar) [*Ma et al.*, 1981; *McSween et al.*, 1979]. Olivine and maskelynite grains are generally 0.25–1.0 mm in diameter, whereas pyroxene grains can be up to several centimeters in size. Pyroxenes occur as high-calcium augite and low-calcium pigeonite (both more magnesian than most shergottites), olivine composition is intermediate to forsteritic (~Fo_{74}), and maskelynite grains are zoned from An_{54} to An_{45} [*McSween et al.*, 1979]. Minor to trace amounts of chromite, ilmenite, troilite, and whitlockite are also present. Shock effects are manifested as undulatory extinction and deformation twinning in the pyroxenes, pockets of olivine vitrophyre, and conversion of plagioclase feldspar to maskelynite [*McSween et al.*, 1979]. The crystallization age of ALH77005 has been estimated at 187 ± 12 Ma [*Shih et al.*, 1982] or 154 ± 6 Ma [*Jagoutz*, 1989].

Zagami is a basaltic shergottite. Our sample was acquired from a private collector, who was also the source for Zagami samples currently held by the University of New Mexico [e.g., *McCoy et al.*, 1992]. This sample is a triangular slice, measuring approximately 2.0 × 2.0 × 0.6 cm. Zagami is approximately 73% pyroxene, 20% maskelynite, and 5% mesostasis and minor phases [*Stolper and McSween*, 1979; *McCoy et al.*, 1992; *Treiman and Sutton*, 1992]. Grain sizes range from 0.19 to 0.36

mm within the meteorite. Pyroxenes in Zagami are augite and pigeonite, in roughly equal amounts, and maskelynite has a composition of ~An_{50}. Shock effects are observed not only in the transformation of plagioclase to maskelynite, but are manifested in the pyroxenes as fracturing and undulatory or patchy extinction [*Stolper and McSween*, 1979]. The crystallization age of Zagami is uncertain, having been interpreted to be as long ago as 1.3 Ga [*Shih et al.*, 1982; *Wooden et al.*, 1982] or as recently as 180 Ma [*Jones*, 1986].

EET79001 is also a basaltic shergottite, similar in composition to Zagami. The meteorite contains two lithologies (A and B) which have differing grain sizes. Our sample of this meteorite, from the Antarctic Meteorite Collection at Johnson Space Center, is from the A lithology, and consists of six pieces. The largest piece is 1.75 × 0.75 × 0.5 cm, two pieces are approximately 1.0 × 0.75 × 0.5 cm, and the three smallest pieces are roughly equant, approximately 0.5 cm on a side. Grain sizes in the A lithology range from approximately 2.7 to 3.6 mm. Pyroxene comprises 70.8% of the meteorite (59.3% pigeonite, 6.1% augite, and 5.4% orthopyroxene), while 17.1% is maskelynite (~An_{60}) and 8.9% is olivine [*Steele and Smith*, 1982; *McSween and Jarosewich*, 1983; *McSween*, 1985]. Minor oxide phases such as titanomagnetite, ilmenite, and chromite contribute 3.0%, and the remainder of the meteorite (0.3%) is minor to trace amounts of mesostasis, sulfides, and phosphates. Orthopyroxene, olivine, and chromite are xenocrysts, apparently of a lherzolitic shergottite similar to ALH77005, within a basaltic shergottite host rock. Shock effects in this meteorite are similar to those observed in Zagami; plagioclase feldspar has been transformed into maskelynite, and pyroxene grains contain planar fractures, exhibit mechanical twinning, and display patchy extinction. The proposed crystallization age of EET79001 is also similar to the older age for Zagami, in the range of 1.0–1.3 Ga [*Shih et al.*, 1982].

3. Experimental Methods

3.1. Sample Preparation and Data Acquisition

The vibrational emission technique is ideal for bulk meteorite analysis because it is nondestructive and minimal sample preparation is required relative to many methods of geological analysis; for example, some of the meteorite samples were cut, by necessity, but a cut surface is not required. No samples were polished, slides are not required, nor must the sample be crushed or powdered. Mineral standards used in this study are from the Thermal Emission Spectrometer Laboratory's mineral library and are pure particulate samples, with grain sizes between 710 μm and 2 mm.

The spectrometer used in this study is a Mattson Cygnus 100 Fourier transform infrared (FTIR) interferometric spectrometer which has been modified to measure emitted sample radiance (a detailed description of the emission technique and the Arizona State University (ASU) spectrometer is provided by *Ruff et al.* [1997]). The sample chamber is located within a glovebox that is external to the spectrometer; both the glovebox and the spectrometer are constantly purged to remove atmospheric H_2O and CO_2. Data for this study were collected over the wavelength range of 2000–400 cm^{-1} (5–25 μm) at a spectral sampling of 2 cm^{-1}; however, spectral data will be shown from 1400 to 400 cm^{-1} (~7–25 μm) because there are no silicate features in the 2000–1400 cm^{-1} region, and carbonate features were not observed because carbonate is not present in any of the meteorites. Samples were heated to 80°C to improve signal to noise, and this temperature was maintained throughout data acquisition. The radiance of a 1 cm spot on each sample was measured. With this placement, a large portion of the sample surface is observed, and the potential for observing a nonrepresentative area of the sample is reduced. Where possible, multiple surfaces were measured, and no significant spectral variations were observed. For each sample, 260 scans were collected over approximately 7 min and averaged to produce a single spectrum. Raw radiance data were converted to emission spectra following the method of *Christensen and Harrison* [1993]. Sources of error in the acquisition of this data are described by *Ruff et al.* [1997]; the total instrument-derived error for any given spectrum in this study is approximately 2–5%.

3.2. Linear Deconvolution

In addition to qualitative observations of spectral feature position, we use a linear deconvolution algorithm to calculate the relative spectral contributions of end-member minerals to a sample spectrum and arrive at an approximate determination of the sample's mineralogic composition. Linear spectral deconvolution has been used in both the VNIR and thermal infrared [*Johnson et al.*, 1983; *Gillespie*, 1992; *Thomson and Salisbury*, 1993; *Ramsey*, 1996b]. This technique is based on the principle that the energy emitted from a rock surface is equivalent to the linear addition of the emitted energy of each component mineral in proportion to its observed areal percentage. The assumption of linear addition has been shown to be valid for grain sizes >65 μm, as discussed below.

The variations in spectral contrast that result from differing grain sizes are a well-known effect in spectroscopic studies. Numerous studies have shown that as particle size decreases, spectral contrast decreases uniformly across the spectrum as well [*Lyon*, 1964; *Aronson et al.*, 1966; *Vincent and Hunt*, 1968; *Aronson and Emslie*, 1973; *Salisbury and Eastes*, 1985; *Salisbury and Wald*, 1992; *Moersch and Christensen*, 1995; *Mustard and Hays*, 1997]. Therefore the spectrum of a mixture composed of small grains will have less spectral contrast than a mixture composed of relatively larger grains, and the deconvolution algorithm may then be used to estimate the grain size(s) represented by a sample's spectrum. This assumption of decreasing spectral contrast with decreasing grain size was shown to be valid down to grain sizes of about 65 μm in a study using quartz [*Moersch and Christensen*, 1995]; below this threshold, scattering effects between small grains produced nonuniform absorption band variations. A similar study by *Mustard and Hays* [1997] found that the majority of nonlinear effects in olivine occurred at grain sizes <25 μm; however, transparency features are apparent in the spectra at grain sizes between 25 and 65 μm; therefore we have intentionally maintained sample grain sizes greater than 65 μm.

We have used the linear deconvolution algorithm of *Ramsey* [1996a, b], in which spectra of pure minerals provide end-members for the model. The algorithm uses a least squares fit to deconvolve a rock spectrum into percentages of end-member mineral spectra, and estimates the average (root-mean-square, or rms) error in the fit. While an rms error is provided by the algorithm for each analysis, we find that it is most useful in determining the best fit to a single sample over several analyses. Although the spectral match to one sample may yield a lower rms error than in the case of another sample, there is no correlation with more accurate determinations of modal percentages. For example, the rms error in the

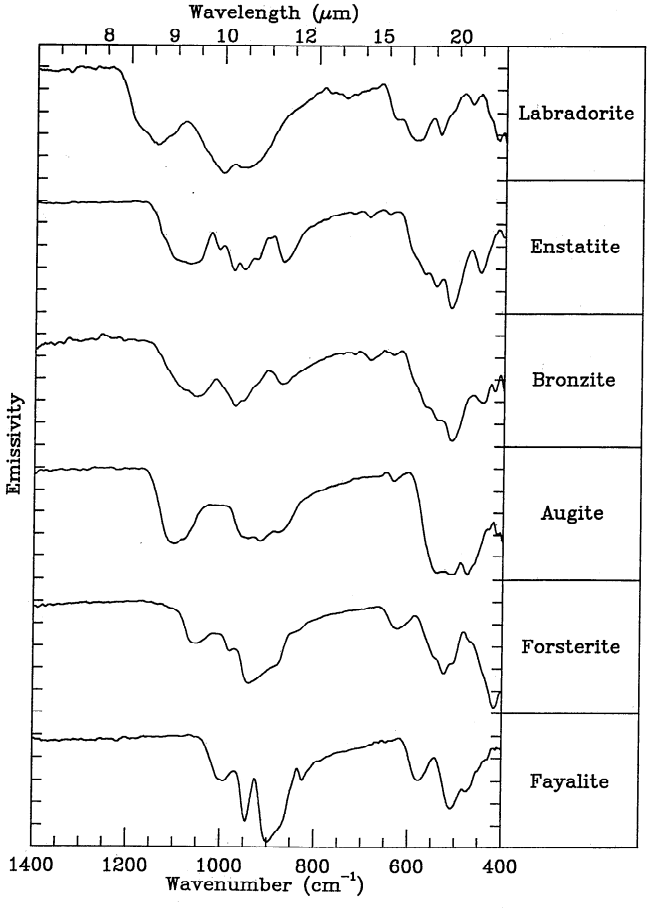

Figure 1. Middle infrared emission spectra of representative end-member minerals. Spectra are normalized for comparison.

EET79001 spectral fit is 0.0086 (0.08%), while for Zagami, it is 0.0113 (0.11%); however, the Zagami model-derived mineral percentages are much more accurate than those determined for EET79001, as discussed below. Additionally, the rms error is an average over the whole spectrum, which is not very useful for evaluating the fit around the absorption features. A more useful assessment of model fit is shown by a spectrum of the residual error (measured minus model) for each fit. In addition to showing the residual error spectra, we will discuss the difference between the published or known percentage of a given mineral in a sample and the value returned by the best fit of the linear deconvolution model. If a mineral mode in a meteorite has a published value of 46% and the model returns a value of 49%, we will refer to this difference as an overestimation of 3%.

The ability to determine accurately end-member modes using the algorithm is dependent on mineral abundance, composition, and limitations inherent in the data, such as spectral resolution and noise [*Ramsey*, 1996a, b]. As the modal abundance of a mineral in the sample increases, uncertainty in the model determination decreases, due to the increasing band depth of spectral features relative to noise in the data. Thus the model-determined modes of minerals present in low abundances (~3–5%) have the largest uncertainties. Minor and trace constituents such as mesostasis and oxides cannot be modeled in most situations, typically because their contributions to the bulk spectrum are unresolvable. Because the model iterates until the calculated modes sum to ~100%, error in the model results will include the total percentage of minor constituents. For example, if a rock has 3% minor and trace constituents that cannot be modeled, some mineral(s) that provides the closest fit will have an elevated mode in the final calculation so that the summation will approach 100%. *Ramsey* [1996b] deconvolved six 4-mineral mixtures, which included modal percentages as low as 5 and 10%. In the six mixtures, there were 10 components at 5 or 10% modal abundance. Model error in determining the minerals present at the 5% level ranged between 0.7 and 5.0%. Error in determining mineral modes at the 10% level was slightly better, ranging between 0.4 and 4.0% [*Ramsey*, 1996b].

End-member mineral composition must also be considered when evaluating deconvolution results. It is rare that an end-member provided as a model input will have the exact same composition as the mineral in the bulk sample, especially when the mineral has a composition within a solid solution series. As a result, spectral band depths may vary, and there may be small variations (2–10 cm^{-1}) in absorption feature position [*Hamilton and Christensen*, 1997]. Once the primary minerals in a sample have been isolated using the linear deconvolution algorithm, it then may be useful to run the algorithm with several additional spectra which represent the spectral variability of those minerals in order to refine the spectral fit of the model result. The best spectral fit would be determined by comparing the rms error for each run of a sample and selecting the fit with the lowest rms and residual error.

3.3. End-Member Selection

The meteorite spectra were initially compared to spectra in the ASU mineral library, which contains over 150 pure mineral spectra representing most of the major mineral groups. These initial analyses identified several each of pyroxenes (enstatite, bronzite, diopside, augite, and hedenbergite), olivines (forsterite and fayalite), and plagioclase feldspars (albite, labradorite, and anorthite) (Figure 1), as well as terrestrial maskelynite (shown in Figure 3), which were used in subsequent analyses. The success of the linear deconvolution method at fitting the correct minerals, while eliminating minerals present in the library but not in the meteorites, provides strong support for this technique as a tool for uniquely identifying rock mineralogy.

Unfortunately, we were not able to include a pigeonite end-member due to the difficulty of obtaining a pure, uninverted sample of sufficient grain size; the effects of this omission on model results are discussed below. We were also unable to provide an end-member spectrum of shocked pyroxene. The maskelynite spectrum is of a single piece of shocked anorthosite from near the Manicouigan impact crater in Ontario, Canada. The composition of Manicouigan maskelynite is approximately An_{50} [*Bunch et al.*, 1967; *Arndt et al.*, 1982]. We are unable to determine if or how closely the spectrum of this sample resembles the spectral equivalent of maskelynite in these meteorites because we have not produced mineral separates from the meteorites. *Nash and Salisbury* [1991] examined the middle infrared spectral characteristics of fused plagioclase, but we are not confident that we can apply their results to our terrestrial or meteorite samples because (1) their sample grain size was <65 μm and (2) fused minerals are significantly different in their physical and spectral character than shocked minerals [*Bunch et al.*, 1967].

Spectral absorptions of some pure minerals exhibit greater spectral contrast (are deeper) than absorptions in the spectra

of the rocks they occur in. In order to account for differences in spectral band depth related to this effect, we have included a blackbody end-member (unit emissivity at all wavelengths) in our analyses. When added to a spectrum, a blackbody end-member reduces spectral contrast uniformly across the spectrum. Thus the deconvolution algorithm can, if necessary, mathematically reduce or eliminate differences in spectral band depth between the end-member mineral spectra and the meteorite spectra.

4. Results

4.1. Spectral Discrimination of Martian Meteorite Lithologies

The vibrational emission spectra of Nakhla, ALH77005, Zagami, and EET79001 are shown in Figure 2. The spectra exhibit similarities in the positions of their reststrahlen bands, indicating gross similarities (mafic to ultramafic) in composition. The positions and relative depths of individual absorptions are distinctly different between each meteorite, however, due to the variations in the abundances and composition of the primary minerals. Zagami and EET79001 look rather similar, which is to be expected because both are basalts, while ALH77005 (lherzolite) and Nakhla (clinopyroxenite) look very different from each other and the Zagami/EET79001 pair. Thus it is possible to discriminate three basic lithologies among these meteorites using gross spectral properties alone.

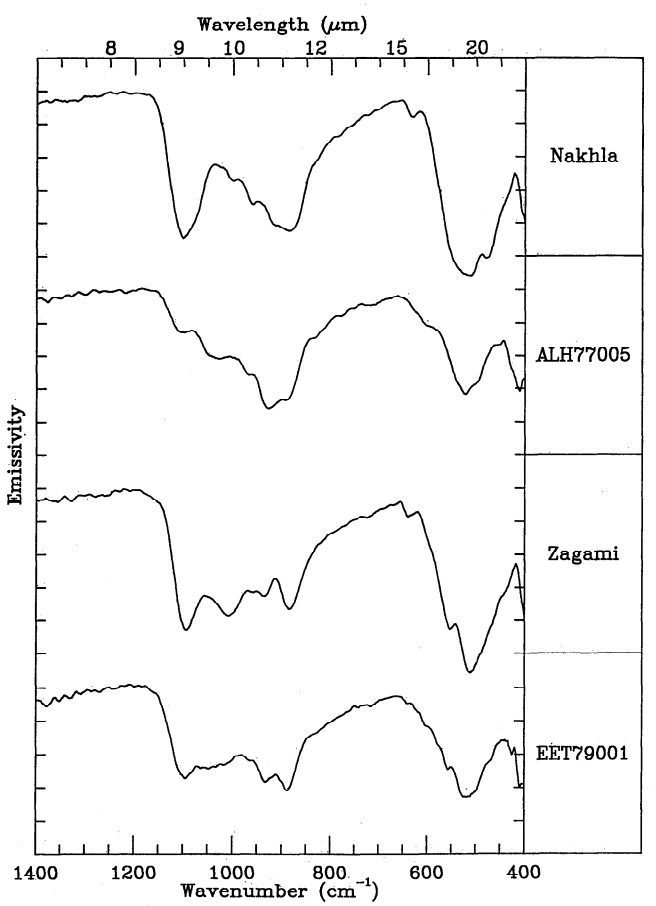

Figure 2. Middle infrared emission spectra of meteorite samples Nakhla, ALH77005, Zagami, and EET79001. Spectra are not normalized, and tick marks represent a $\Delta\varepsilon$ of 0.03.

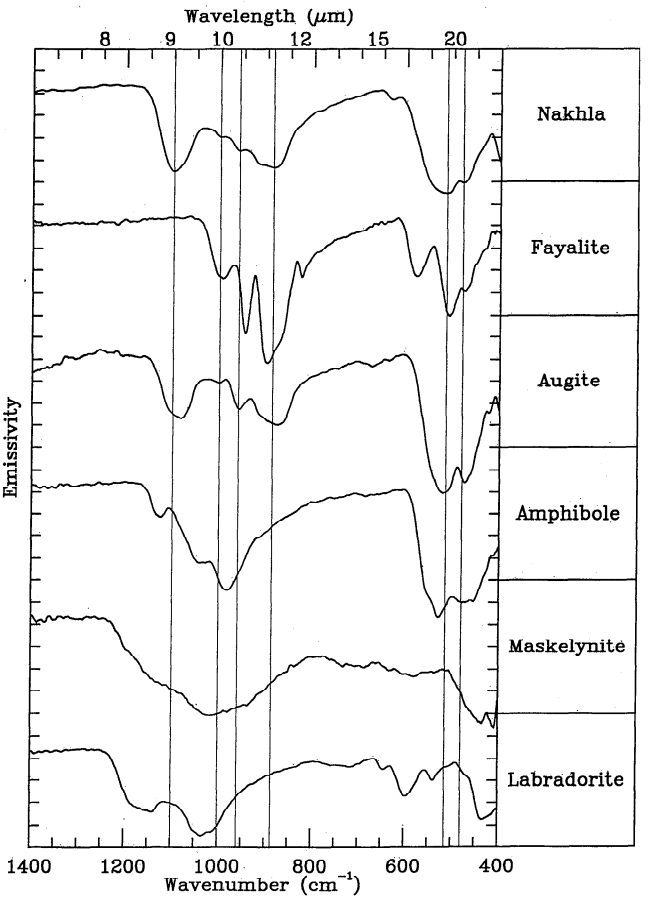

Figure 3. Middle infrared emission spectra of Nakhla and various silicate minerals. Minerals are arranged in order of increasing Si-O tetrahedral polymerization, and each tick represents $\Delta\varepsilon \sim 0.04$. Vertical lines correspond to primary absorption features in the Nakhla spectrum.

More detailed information about meteorite mineralogy can be obtained by comparison of the meteorite spectra with individual mineral spectra. Figure 3 shows the Nakhla spectrum and the spectra of minerals from four of the silicate structural groups. Silicate absorption features in the 1250–800 cm^{-1} range move to longer wavelengths due to changes in the asymmetric Si-O-Si stretching vibrations as a function of decreasing Si-O tetrahedral polymerization [*Walter and Salisbury*, 1989; *Salisbury et al.*, 1991b]. The Nakhla spectrum displays absorption features in the 1250–800 cm^{-1} range that are at wavelengths comparable to features in minerals with relatively low degrees of SiO_4 polymerization, such as amphibole, pyroxene, and olivine. This observation suggests that the meteorites in this study (all having similarly located reststrahlen bands) are dominated by silicate minerals of the chain and isolated tetrahedral structural groups. We can use this comparison to individual mineral groups to show that the three lithologies are fairly closely related, in this case, all representing primarily mafic compositions. The 1250–800 cm^{-1} absorption group in granitic rocks, for example, is typically located at shorter wavelengths [*Lyon*, 1964; *Vincent and Thomson*, 1972; *Vincent et al.*, 1975], due to the abundance of highly polymerized framework silicates such as quartz and feldspar [*Walter and Salisbury*, 1989].

Table 1. Measured and Model-Derived Modal Mineral Abundances for Nakhla, ALH77005, Zagami, and EET79001

	Nakhla[a,b]		ALH77005[c,d]		Zagami[e,f]		EET79001[g]	
Mineral Type	Measured	Model	Measured	Model	Measured	Model	Measured	Model
High-Ca px	74–85	73	11	23 [16]	30–40	37	6	43 [29]
Low-Ca px		11	26	7 [5]	37–40	41	65	14 [10]
Plagioclase	4	8	10 (m)	19 [14]	10–19 (m)	18 (4 m)	17	27 [18]
Olivine	5–18	8	52	51 [46]		4	9	16 [11]
Miscellaneous	3		1		5		3	
Blackbody				[29]				[33]
rms error		0.0067		0.0066		0.0111		0.0093

Low-Ca px category includes orthopyroxene and/or pigeonite; (m) indicates maskelynite. Numbers in brackets are percentages prior to removal of blackbody component. Values are in units of vol %.

[a]R. C. Friedman (personal communication, 1996).
[b]*Bunch and Reid* [1975].
[c]*Ma et al.* [1981].
[d]*McSween et al.* [1979].
[e]*McCoy et al.* [1992].
[f]*Stolper and McSween* [1979].
[g]*McSween and Jarosewich* [1983].

4.2. Results: Determination of Meteorite Mineralogy From Spectral Data

While discrimination of lithology is desirable, more quantitative determinations of meteorite mineralogy can be obtained using the linear deconvolution technique. The results of the linear deconvolution for all four samples are shown in Table 1 and Figure 4. In two cases, the deconvolution algorithm determined that a blackbody component was necessary to match most accurately the measured meteorite spectra. In calculating the final modal mineral percentages for comparison with the published compositions of each meteorite, we removed the blackbody percentage and normalized the mineral endmembers. For the purposes of visual comparison, we show the model spectra with the blackbody component included. Table

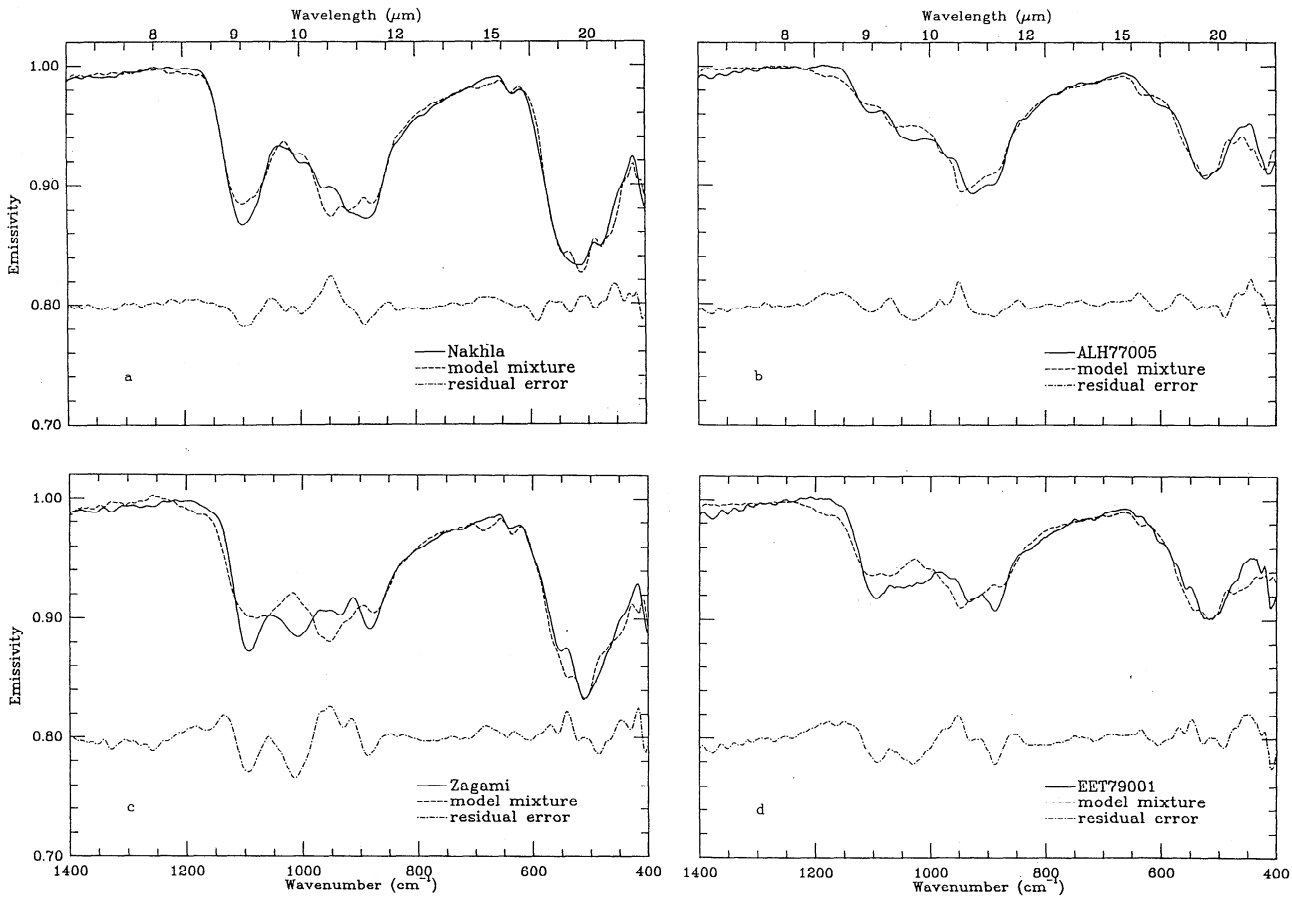

Figure 4. Measured and model-derived meteorite emission spectra: (a) Nakhla, (b) ALH77005, (c) Zagami, and (d) EET79001. Note expanded vertical scale.

Table 2. Compositions of Major Minerals in Meteorite Samples and Arizona State University (ASU) Model End-Members

Mineral	Nakhla[a]	ALH77005[b]	Zagami[c,d]	EET79001[e]	ASU Model End-Members
High-Ca pyroxene	En_{38} Fs_{23} Wo_{39}	En_{52} Fs_{15} Wo_{33}[f]	En_{38} Fs_{28} Wo_{34}[f]	En_{45} Fs_{27} Wo_{28}	En_{50} Fs_{0} Wo_{50}[g] En_{41} Fs_{15} Wo_{44} En_{17} Fs_{33} Wo_{49}[g]
Low-Ca pyroxene		En_{70} Fs_{24} Wo_{6}	En_{53} Fs_{36} Wo_{11}[f]	En_{53} Fs_{36} Wo_{11}[f] En_{67} Fs_{24} Wo_{5}	En_{90} Fs_{9} Wo_{1} En_{77} Fs_{20} Wo_{3}
Feldspar (plagioclase)	An_{27}				An_{3}[g] An_{54} An_{89}[g]
Maskelynite		An_{54-45}	An_{50}	An_{57}[f]	An_{50}
Olivine	Fo_{32}	Fo_{74}		Fo_{72}	Fo_{1-5} Fo_{91}

[a]*Bunch and Reid* [1975].
[b]*McSween et al.* [1979].
[c]*Treiman and Sutton* [1992].
[d]*Stolper and McSween* [1979].
[e]*McSween and Jarosewich* [1983].
[f]Average composition of zoned or multiple crystals.
[g]Not utilized in any of the four best fit model results.

2 compares the composition of minerals in the meteorites to the compositions of the pure end-member minerals.

4.2.1. Nakhla. The deconvolution algorithm produces the best fit using the three primary minerals in this meteorite (augite, fayalite, and plagioclase feldspar) in addition to a small percentage of low-Ca pyroxene (Figure 4a). The best fit modeled mineral percentages match to within approximately 4–11% of the published data for Nakhla (Table 1). Nakhla is classified as a plagioclase-bearing olivine clinopyroxenite according to the International Union of Geological Sciences (IUGS) classification scheme. The spectrally derived mineral modes shift the classification slightly, into the olivine websterite category (Figure 5).

Of the plagioclase end-members provided, the best model fit is produced with a feldspar of intermediate composition (labradorite), while the composition determined by *Berkley et al.* [1980] is closer to An_{25}. However, the spectra of intermediate feldspars are much more similar to each other than they are to albite and anorthite spectra, which exhibit very sharp, distinctive absorptions (S. W. Ruff, personal communication, 1997). Therefore any intermediate composition in the unknown sample is likely to be fit best by a model end-member of the closest intermediate composition. The slight overestimation (4%) of modal plagioclase is within the error of the model and is not of great concern.

The modeled olivine percentage is within the range of observed values (5–18%) (R. C. Friedman, personal communication, 1996). The best model fit is obtained with the more Fe-rich end-member, fayalite (Fo_{1-5}), in agreement with the published olivine composition [*Bunch and Reid*, 1975]. Of the three plagioclase end-members provided (albite, labradorite, and anorthite), the best model fit is produced with the intermediate labradorite which is near the composition measured in Nakhla samples. The 4% difference between the known and modeled modal plagioclase is within the uncertainty associated with the model calculation.

The total modeled pyroxene abundance (84%) was determined to be within the range of observed values (74–85%) measured by Friedman and co-workers (R. C. Friedman, personal communication, 1996). Because the modeled olivine

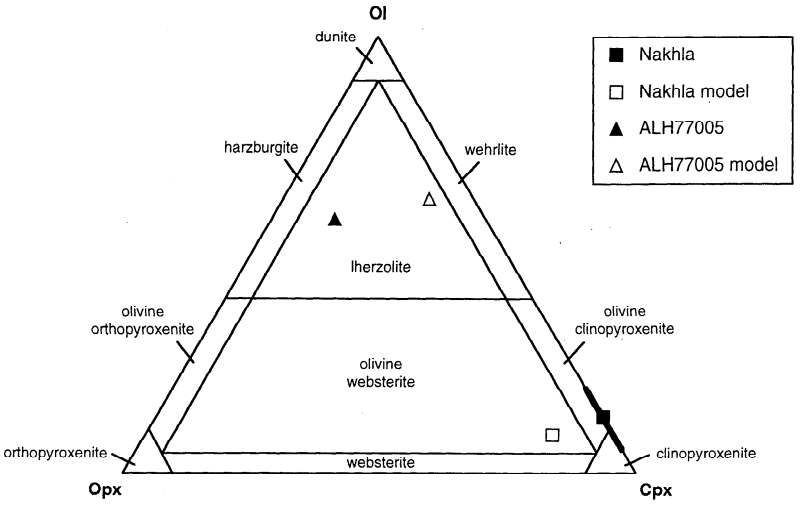

Figure 5. IUGS classification diagram for ultramafic rocks. Measured and modeled modal compositions of Nakhla and ALH77005 are plotted. The heavy line represents the compositional variability among Nakhla samples.

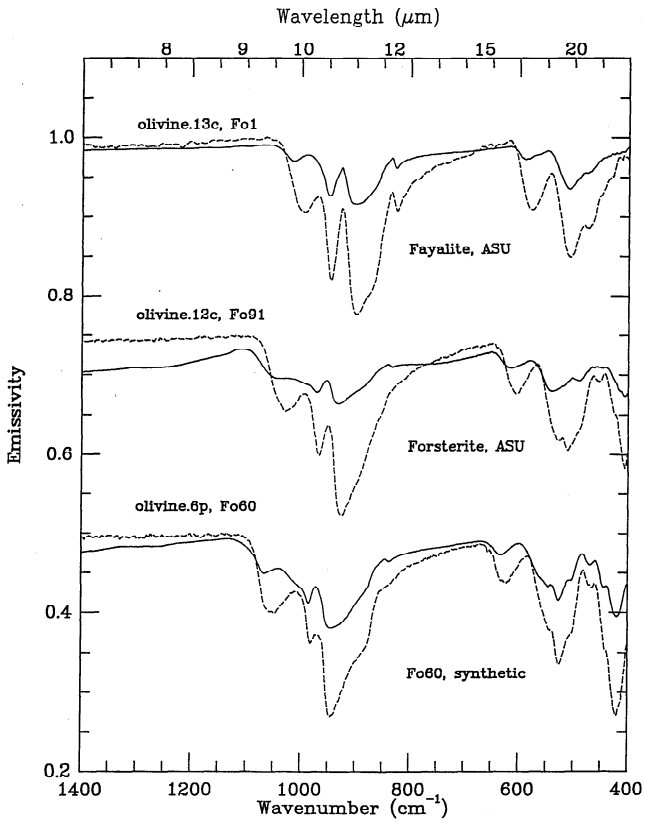

Figure 6. Spectra of laboratory olivines and a synthetic spectrum of an intermediate olivine composition. Solid lines are spectra from *Salisbury et al.* [1991b], and dashed lines are Arizona State University (ASU) samples. The synthetic spectrum was produced by a weighted average of the ASU forsterite and fayalite samples to approximate a composition of Fo_{60}.

mode was at the low end of the range of observed modes, we expected an increase in total pyroxene abundance [*Friedman et al.*, 1994]; this increase was observed, but the best fit model contains low-Ca pyroxene instead of additional augite. We believe that low-Ca pyroxene provides a better mathematical fit than an increase in the high-Ca pyroxene mode due to differences in the relative band depths of the input end-member spectra. The augite end-member (Table 2) we used is the closest composition in our library to the composition in Nakhla. The appropriateness of this selection was verified by a test deconvolution which included several augite spectra representing various compositions; this augite sample provided the best match to Nakhla, producing fits with the lowest rms and residual errors. However, the compositions of our augite and the augite in Nakhla still differ and may be a source of error in the spectral fit. Additionally, this augite has band depths in the 700–400 cm^{-1} region that are much lower in emissivity (ε) than the average emissivity of the absorptions in the 1200–800 cm^{-1} region (Figure 3). In contrast, the same two absorption groups in the spectrum of Nakhla do not have significantly different average depths ($\Delta\varepsilon \sim 0.02$). Therefore, in order to mathematically decrease the emissivity difference between the spectrum of Nakhla and the model spectrum, a mineral with similar pyroxene features and low $\Delta\varepsilon$ between absorption groups (enstatite) is used in the final fit instead of augite. This hypothesis was supported by an additional analysis in which the model was restricted to fitting the meteorite spectrum between 1200 and 700 cm^{-1}, thus omitting the effect of features in the 700–400 cm^{-1} region from the determination. The result of this wavenumber-limited analysis was an increase in the determined amount of augite from 73% to 91% (still within the model uncertainty) and a reduction in the modeled abundance of the enstatite end-member to 5%. Although the enstatite end-member was not eliminated, the low percentage calculated approaches the percent error in the model result (which includes instrumental error in the spectra, the model itself, and the 3% of the meteorite that is composed of minor constituents which cannot be modeled). This case exemplifies the need for multiple analyses of a sample once the primary constituents have been identified; in order to achieve the most accurate results possible, the user should include several spectra of each of the primary minerals, examine the rms error variations, and be aware that variations in end-member band depth can influence the accuracy of the model results.

4.2.2. ALH77005. In the case of ALH77005 (Figure 4b), the model accurately retrieved the four primary minerals in the meteorite from the spectral library: olivine, plagioclase, and high- and low-Ca pyroxene. A blackbody component was also included in the model fit; because the end-member and meteorite grain sizes are similar, we determined that the blackbody improved the fit by reducing the spectral contrast of the dominant end-member mineral which has deeper spectral features than the meteorite. Published mineral abundances classify ALH77005 as a plagioclase-bearing lherzolite (Figure 5); model-derived abundances result in the same classification, although with slightly more low-Ca pyroxene. This result is not unexpected due to the fact that ALH77005 is a heterogeneous sample [*McSween et al.*, 1979] and the mineralogy of the surface we examined may differ slightly from previously reported results.

Total olivine content is determined to within 2% of the published mode (Table 1), and the model fit includes both forsterite and fayalite, at 33% and 19%, respectively. The published composition of olivine in ALH77005 is Fo_{74} [*McSween et al.*, 1979], and we believe that the inclusion of both end-members is an approximation of this more intermediate composition. *Salisbury et al.* [1991b] note that the absorption features in olivine spectra display a progressive shift to shorter wavelengths from fayalitic to forsteritic compositions. This shift corresponds to the increasing substitution of Mg for Fe in olivine with the smaller, lighter Mg cations vibrating at higher frequencies. Thus a weighted combination of the end-member spectra should approximate the spectrum of an intermediate composition. Figure 6 shows the spectra of pure end-member olivines from our library, a synthetic intermediate composition derived from the weighted average of the library end-members, and comparison reflectance spectra (inverted for comparison to emissivity) from *Salisbury et al.* [1991b]. Although there are dissimilarities in the pairs of spectra due to differences in the techniques used to acquire the spectra (emission versus biconical reflectance), it is possible to see that the dominant absorption features occur in the same positions in all three pairs of spectra, indicating that the combination of end-member spectra is an adequate approximation of the spectrum of an intermediate composition.

The model overdetermines augite by 12%, possibly in compensation for the missing pigeonite end-member. In the absence of a pigeonite end-member, the model calculates bronzite as the closest possible match to the pigeonite component of the meteorite. Although structurally different from

orthopyroxenes, the pigeonite in the meteorite is close to bronzite in composition; therefore our result suggests that even without a true pigeonite end-member, the end-member spectra can be used in the model to distinguish between high- and low-Ca components and, moreover, determine the general Mg/Fe ratio.

Instead of maskelynite, an intermediate plagioclase (labradorite) provides the best fit to the meteorite spectrum. We believe that this is due to the spectral band depths of the maskelynite sample as compared to the labradorite and meteorite spectra. The 1400–700 cm^{-1} absorption group in maskelynite is higher in emissivity than the same absorption groups in the plagioclase and meteorite spectra. Additionally, the maskelynite spectrum does not display similarly high emissivities in the 800–600 cm^{-1} region as the plagioclase and the meteorite. Because the deconvolution algorithm seeks to mathematically reduce the $\Delta\varepsilon$ between the measured and model spectra, end-members with anomalously high or low emissivity features may not provide the best fit (as in the case of augite, described above). However, in fitting the plagioclase component of the meteorite spectrum, the model determines that an intermediate composition is the best fit, which is in accordance with the known composition of the maskelynite in ALH77005.

4.2.3. Zagami. Model results for Zagami are enigmatic; the best fit model includes the correct minerals and calculates their abundances more accurately than in any other case; however, the spectral match is poor at short wavelengths (Figure 4c). We define "poor" as meaning that the spectral shape of the model does not closely mimic the shape of the measured spectrum, even though the absolute difference in emissivity between the two may not be exceptionally large; e.g., at approximately 1025 cm^{-1}, there is a peak in the spectrum of the model, but the measured spectrum displays a trough.

The best fit is provided by high-Ca pyroxene, low-Ca pyroxene, intermediate plagioclase feldspar (labradorite), and a small percentage (2%) of terrestrial maskelynite. The percentages of these minerals are determined to within 5% of the published values, and in the best case, augite is determined to within 1% of its actual mode in the meteorite. The small percentage of maskelynite is suspect due to uncertainties in the detectability of minor constituents, as discussed above. Based on the basalt tetrahedron of *Yoder and Tilley* [1962], Zagami is classified as a pyroxene-rich (tholeiitic) basalt, and the model-derived percentages result in the same classification. At this time, we consider the misfit of the model spectrum to the measured spectrum a result of the omission of a pigeonite end-member or possibly a result of strong shock effects in the pyroxenes or plagioclase. The published modal percentage of pigeonite in this sample is higher than that in either Nakhla or ALH77005, and we expect this greater abundance to result in a stronger spectral contribution from the pigeonite end-member. As a result, the contribution of the pigeonite spectrum to the meteorite spectrum will be enhanced, and bronzite will fail to fit any of the spectral features of the meteorite. We have not yet been able to acquire a sample of shocked pyroxene that would allow a spectral comparison. We suspect that the mismatch is less likely to be related to the shock effects in plagioclase because the model consistently uses unshocked plagioclase in this and other samples to best fit the spectral data.

4.2.4. EET79001. Although the model analysis of EET79001 included the correct minerals (pyroxene and feldspar), the difference between the measured and modeled mineral abundance varied between 8% (plagioclase) and 47% (low-Ca pyroxene), and the model produced a spectrum that did not provide a good fit to the measured spectrum. The inaccuracy of the modeled mineral abundances changes the EET79001 rock type from pyroxene-rich (tholeiitic) basalt to olivine tholeiite [*Yoder and Tilley*, 1962]. EET79001 is nearly 60% pigeonite, and we believe that, as in the case of Zagami, our lack of a pure pigeonite end-member is resulting in error in the model results. Because the meteorite spectrum will be dominated by pigeonite-specific features at this high abundance, the model can no longer successfully substitute low-Ca bronzite and thus overestimates the remaining minerals in the final summation. As in the case of ALH77005, the blackbody component included in the model fit improves the fit by reducing the spectral contrast of the end-members with deep spectral features. The model results in the case of EET79001 emphasize the need for a complete library of minerals and user verification of model results in order to ensure the utmost accuracy in using this (or any) model for the determination of modal mineralogy from bulk sample spectra.

5. Application to Martian Spectroscopy

Martian spectra acquired from orbit should exhibit similar spectral contrasts to laboratory spectra, especially in regions on the Martian surface where the surface is composed of coarse, active materials, such as dark regions like Syrtis Major or dune fields, and in locally homogeneous (at the 3 km scale) regions. In many locations the area observed within a TES footprint will include a variety of compositions and/or grain sizes; in these circumstances, spectral contrast may be reduced, and researchers will certainly need to further analyze deconvolution results using their geological knowledge of naturally coexisting minerals and grain size effects. If a significant amount of dust in an area results in a reduction in spectral contrast, the dust may be considered a component of a mixture that also includes rocky or coarse particulate materials. The positions and relative band depths of mineralogical features will not be different, however, and these characteristics are what linear deconvolution calculations are based upon. If miniaturized thermal emission spectrometers are sent to the surface of Mars on landers and/or rovers in the future, spectral contrasts will also approximate those obtained with laboratory measurements, and complex mixtures over the smaller (centimeter to meter scale) observational areas may be less common.

6. Conclusions

1. Upon visual comparison of the spectra of Nakhla, ALH77005, Zagami, and EET79001 to mineral spectra and to each other, we are able to determine that the meteorite spectra represent three mafic lithologies. The positions of the reststrahlen bands suggest that mafic minerals dominate all four samples, and the similarity in absorption position and shape in the spectra of Zagami and EET79001 suggests that these two meteorites represent a single lithology. This result suggests that, at a minimum, in remote sensing situations, we will be able to distinguish surface lithologies using middle-infrared emission spectra.

2. In three out of four cases, linear deconvolution analyses determine modal mineral abundances in the meteorites to within 3–19% of published modes. As a result, we can achieve more quantitative information and classify these mafic and

ultramafic rock types on the basis of linear deconvolution of their thermal infrared spectra.

3. The lack of a pure pigeonite end-member may be a significant source of error in one of our model determinations. In Nakhla, ALH77005, and Zagami, where pigeonite is less than ~37% of the modal composition of the meteorite, the model fits low-Ca bronzite as a substitute for pigeonite. When the modal abundance of pigeonite exceeds ~37%, the model spectral fit is poor in terms of matching all spectral band shapes. Because pigeonite is clearly important to the accuracy of the model results in these cases, our spectral library must be augmented to include a natural or synthetic pigeonite for comparison to Martian spectra (synthesis of several pigeonite compositions has been initiated). There are no end-member spectra available to represent mesostasis and/or minor constituents; therefore errors (~5% in these meteorites) will always exist in the determined mode of any mineral(s) which have spectral features most closely resembling those of minor components. Plagioclase modes are commonly overestimated by 6–18%, probably due to the broad spectral features which characterize the majority of the intermediate plagioclase spectrum relative to most silicates and make it a suitable substitute for subtle spectral contributions from minor constituents, or in cases where a given end-member is not of exactly the same composition as the mineral in the sample (e.g., solid solution series minerals).

4. We are currently unable to assess quantitatively the effects of shock on the spectral features of plagioclase and pyroxene. We assume that some portion of the anomalous results in our study are attributable to unaccounted-for shock effects. These effects are clearly important, and in the future we plan to prepare mineral separates from the EET79001 sample so that we may study the spectral characteristics of the shocked minerals independently.

Acknowledgments. V.E.H. and P.R.C. were supported by NASA's Planetary Geology and Geophysics Program and the Mars Global Surveyor Science Office. V.E.H. is also supported by a National Physical Science Consortium Fellowship including stipend support from the Jet Propulsion Laboratory. H.Y.M. is supported by JPL contract I01-2-0792-057. We gratefully acknowledge the Center for Antarctic Meteorite Studies at JSC for providing us with ALH77005 and EET79001 samples. The National Museum of Natural History, Smithsonian Institution provided sample USNM 426 (Nakhla) as well as bronzite sample NMNH-93527. We would also like to thank M. S. Ramsey for the linear deconvolution algorithm, as well as several conversations regarding its application to this study, and Don Anderson (Arizona State University) for the software used in nondeconvolution spectral analyses. Finally, the authors thank T. L. Roush and J. F. Mustard for their time and thorough reviews, which led to several valuable clarifications in the manuscript.

References

Adams, J. B., Lunar and Martian surfaces: Petrologic significance of absorption bands in the near-infrared, *Science*, *159*, 1453–1455, 1968.

Arndt, J., W. Hummel, and I. Gonzalez-Cabeza, Diaplectic Labradorite glass from the Manicouagan impact crater, I, Physical properties, crystallization, structural and genetic implications, *Phys. Chem. Miner.*, *8*, 230–239, 1982.

Aronson, J. R., and A. G. Emslie, Spectral reflectance and emittance of particulate materials, 2, Application and results, *Appl. Opt.*, *12*, 2573–2584, 1973.

Aronson, J. R., A. G. Emslie, and H. G. McLinden, Infrared spectra from particulate surfaces, *Science*, *152*, 345–346, 1966.

Becker, R. H., and R. O. Pepin, The case for a Martian origin of the shergottites: Nitrogen and noble gases in EETA79001, *Earth Planet. Sci. Lett.*, *69*, 225–242, 1984.

Berkley, J. L., K. Keil, and M. Prinz, Comparative petrology and origin of Governador Valadares and other nakhlites, *Proc. Lunar Planet. Sci. Conf., XI*, 1089–1102, 1980.

Bishop, J., C. Pieters, J. Mustard, S. Pratt, and T. Hiroi, Spectral analyses of ALH84001, a meteorite from Mars, *Meteoritics*, *29*, 444–445, 1994.

Bogard, D. D., L. E. Nyquist, and P. Johnson, Noble gas contents of shergottites and implications for the Martian origin of SNC meteorites, *Geochim. Cosmochim. Acta*, *43*, 1723–1739, 1984.

Bunch, T. E., and A. M. Reid, The nakhlites, 1, Petrography and mineral chemistry, *Meteoritics*, *10*, 303–315, 1975.

Bunch, T. E., A. J. Cohen, and M. R. Dence, Natural terrestrial maskelynite, *Am. Mineral.*, *52*, 244–253, 1967.

Christensen, P. R., The spatial distribution of rock on Mars, *Icarus*, *68*, 217–238, 1986.

Christensen, P. R., and S. T. Harrison, Thermal infrared emission spectroscopy of natural surfaces: Application to desert varnish coatings on rocks, *J. Geophys. Res.*, *98*, 19,819–19,834, 1993.

Christensen, P. R., et al., Thermal emission spectrometer experiment: The Mars Observer Mission, *J. Geophys. Res.*, *97*, 7719–7734, 1992.

Erard, S., J.-P. Bibring, and Y. Langevin, Determination of spectral units in the Syrtis Major–Isidis Planitia region from Phobos/ISM observations (abstract), *Lunar Planet. Sci.*, *XX*, 327, 1990.

Friedman, R. C., T. J. McCoy, and G. J. Taylor, Constraints on the physical details of Nakhlite formation (abstract), *Lunar Planet. Sci.*, *XXV*, 391, 1994.

Gale, N. H., J. W. Arden, and R. Hutchison, The chronology of the Nakhla achondritic meteorite, *Earth Planet. Sci. Lett.*, *26*, 195–206, 1975.

Gillespie, A. R., Spectral mixture analysis of multispectral thermal infrared images, *Remote Sens. Environ.*, *42*, 137–145, 1992.

Hamilton, V. E., and P. R. Christensen, Interpreting the origins and evolutions of Martian basalts from pyroxene composition, II, Vibrational spectroscopy of clinopyroxenes and terrestrial basaltic rocks (abstract), *Lunar Planet. Sci.*, *XXVIII*, 499–500, 1997.

Hapke, B., *Theory of Reflectance and Emission Spectroscopy*, 455 pp., Cambridge Univ. Press, New York, 1993.

Hunt, G. R., and L. M. Logan, Variation of single particle mid-infrared emission spectrum with particle size, *Appl. Opt.*, *11*, 142–147, 1972.

Hunt, G. R., and R. K. Vincent, The behavior of spectral features in the infrared emission from particulate surfaces of various grain sizes, *J. Geophys. Res.*, *73*, 6039–6046, 1968.

Ikeda, Y., Petrography and petrology of the ALH77005 shergottite, *Proc. NIPR Symp. Antarct. Meteorites*, *7*, 9–29, 1994.

Jagoutz, E., Sr and Nd isotopic systematics in ALHA77005: Age of shock metamorphism in shergottites and magmatic differentiation on Mars, *Geochim. Cosmochim. Acta*, *53*, 2429–2441, 1989.

Jagoutz, E., and H. Wänke, Sm-Nd and Rb-Sr studies on Shergotty meteorite, *Lunar Planet. Sci.*, *16*, suppl. A, 15–16, 1985.

Johnson, P. E., M. O. Smith, S. Taylor-George, and J. B. Adams, A semiempirical method for analysis of the reflectance spectra of binary mineral mixtures, *J. Geophys. Res.*, *88*, 3557–3561, 1983.

Jones, J. H., The youngest meteorites, 1, A 180 m.y. igneous age for the shergottites—The constraint of petrography (abstract), *Lunar Planet. Sci.*, *16*, 406–407, 1985.

Jones, J. H., A discussion of isotopic systematics and mineral zoning in the shergottites: Evidence for a 180 m.y. igneous crystallization age, *Geochim. Cosmochim. Acta*, *50*, 969–977, 1986.

Lyon, R. J. P., Evaluation of infrared spectrophotometry for compositional analysis of lunar and planetary soils, II, Rough and powdered surfaces, *NASA Conf. Rep.*, *CR-100*, 1964.

Ma, M.-S., J. C. Laul, and R. A. Schmitt, Complementary rare earth element patterns in unique achondrites, such as ALHA77005 and shergottites, and in the earth, *Proc. Lunar Planet. Sci. Conf., 12th*, 1349–1358, 1981.

McCoy, T. J., G. J. Taylor, and K. Keil, Zagami: Product of a two-stage magmatic history, *Geochim. Cosmochim. Acta*, *56*, 3571–3582, 1992.

McKay, D. S., E. K. Gibson Jr., K. L. Thomas-Keprta, H. Vali, C. S. Romanek, S. J. Clemett, X. D. F. Chillier, C. R. Maechling, and R. N. Zare, Search for past life on Mars: Possible relic biogenic activity in martian meteorite ALH84001, *Science*, *273*, 924–930, 1996.

McSween, H. Y., Jr., SNC meteorites: Are they martian rocks?, *Geology*, *12*, 3–6, 1984.

McSween, H. Y., Jr., SNC meteorites: Clues to Martian petrologic evolution?, *Rev. Geophys.*, *23*, 391–416, 1985.

McSween, H. Y., Jr., What we have learned about Mars form SNC meteorites, *Meteoritics*, *29*, 757–779, 1994.

McSween, H. Y., Jr., and E. Jarosewich, Petrogenesis of the Elephant Moraine A79001 meteorite: Multiple magma pulses on the shergottite parent body, *Geochim. Cosmochim. Acta*, *47*, 1501–1513, 1983.

McSween, H. Y., Jr., L. A. Taylor, and E. M. Stolper, Allan Hills 77005: A new meteorite type found in Antarctica, *Science*, *204*, 1201–1203, 1979.

Moersch, J. E., and P. R. Christensen, Thermal emission from particulate surfaces: A comparison of scattering models with measured spectra, *J. Geophys. Res.*, *100*, 7465–7477, 1995.

Mustard, J. F., and J. E. Hays, Effects of hyperfine particles on reflectance spectra from 0.3 to 25 microns, *Icarus*, *125*, 145–163, 1997.

Mustard, J. F., and J. M. Sunshine, Seeing through the dust: Martian crustal heterogeneity and links to the SNC meteorites, *Science*, *267*, 1623–1626, 1995.

Mustard, J. F., J.-P. Bibring, S. Erard, E. M. Fischer, J. W. Head, S. Hurtrez, Y. Langevin, C. M. Pieters, and C. J. Sotin, Interpretation of spectral units of Isidis–Syrtis Major from ISM–Phobos-2 observations (abstract), *Lunar Planet. Sci.*, *XXI*, 835–836, 1990.

Mustard, J. F., S. Erard, J.-P. Bibring, J. W. Head, S. Hurtrez, Y. Langevin, C. M. Pieters, and C. J. Sotin, The surface of Syrtis Major: Composition of the volcanic substrate and mixing with altered dust and soil, *J. Geophys. Res.*, *98*, 3387–3400, 1993.

Nakamura, N., D. M. Unruh, M. Tatsumoto, and R. Hutchison, Origin and evolution of the Nakhla meteorite inferred from the Sm-Nd and U-Pb systematics and REE, Ba, Sr, Rb abundances, *Geochim. Cosmochim. Acta*, *46*, 1555–1573, 1982.

Nash, D. B., and J. W. Salisbury, Infrared reflectance spectra (2.2–15 μm) of plagioclase feldspars, *Geophys. Res. Lett.*, *18*, 1151–1154, 1991.

Nyquist, L. E., J. Wooden, B. Bansal, H. Wiesmann, and C.-Y. Shih, Sr and Nd isotopic systematics of EETA79001, *Meteoritics*, *19*, 284, 1984.

Palluconi, F. D., and H. H. Kieffer, Thermal inertia mapping of Mars from 60°S to 60°N, *Icarus*, *45*, 415–426, 1981.

Ramsey, M. S., Object detection utilizing a linear retrieval algorithm for thermal infrared imagery, in *Proceedings of the Second International Airborne Remote Sensing Conference, San Francisco, CA*, vol. 2, pp. 559–569, Environ. Res. Inst. of Mich., Ann Arbor, 1996a.

Ramsey, M. S., Quantitative analysis of geological surfaces: A deconvolution algorithm for midinfrared remote sensing data, Ph.D. dissertation, 276 pp., Ariz. State Univ., Tempe, 1996b.

Roush, T. L., D. L. Blaney, and R. B. Singer, The surface composition of Mars as inferred from spectroscopic observations, in *Remote Geochemical Analysis: Elemental and Mineralogical Composition*, edited by C. Pieters and P. Englert, pp. 367–394, Cambridge Univ. Press, New York, 1993.

Ruff, S. W., P. R. Christensen, P. W. Barbera, and D. L. Anderson, Quantitative thermal emission spectroscopy of minerals: A technique for measurement and calibration, *J. Geophys. Res.*, *102*, 14,899–14,913, 1997.

Salisbury, J. W., and J. W. Eastes, The effect of particle size and porosity on spectral contrast in the mid-infrared, *Icarus*, *64*, 586–588, 1985.

Salisbury, J. W., and A. Wald, The role of volume scattering in reducing spectral contrast of reststrahlen bands in spectra of powdered minerals, *Icarus*, *96*, 121–128, 1992.

Salisbury, J. W., D. M. D'Aria, and E. Jarosewich, Mid-infrared (2.5–13.5 μm) reflectance spectra of powdered stony meteorites, *Icarus*, *92*, 280–297, 1991a.

Salisbury, J. W., L. S. Walter, N. Vergo, and D. M. D'Aria, *Infrared (2.1–25 μm) Spectra of Minerals*, 267 pp., Johns Hopkins Univ. Press, Baltimore, Md., 1991b.

Shih, C.-Y., L. E. Nyquist, D. D. Bogard, G. A. McKay, J. L. Wooden, B. M. Bansal, and H. Wiesmann, Chronology and petrogenesis of young achondrites, Shergotty, Zagami, and ALHA77005: Late magmatism on a geologically active planet, *Geochim. Cosmochim. Acta*, *46*, 2323–2344, 1982.

Singer, R. B., The dark materials on Mars, II, New mineralogic interpretations from reflectance spectroscopy and petrologic implications, *Lunar Planet. Sci.*, *XI*, 1048–1050, 1980a.

Singer, R. B., and T. L. Roush, Analysis of Martian crustal petrology, *Am. Astron. Soc. Bull.*, *17*, 737, 1985.

Singer, R. B., R. N. Clark, and P. D. Owensky, Mars: New regional near-infrared spectrophotometry (0.65–2.50 μm) obtained during the 1980 apparition, *Bull. Am. Astron. Soc.*, *12*, 680, 1980b.

Soderblom, L. A., The composition and mineralogy of the Martian surface from spectroscopic observations: 0.3 μm to 50 μm, in *Mars*, edited by H. H. Kieffer, B. M. Jakosky, C. W. Snyder, and M. S. Matthews, pp. 557–593, Univ. of Ariz. Press, Tucson, 1992.

Steele, I. M., and J. V. Smith, Petrography and mineralogy of two basalts and olivine-pyroxene-spinel fragments in achondrite EETA79001, *Proc. Lunar Planet. Sci. Conf. 13th*, Part 1, *J. Geophys. Res.*, *87*, suppl., A375–A384, 1982.

Stolper, E. M., and H. Y. McSween Jr., Petrology and origin of the shergottite meteorites, *Geochim. Cosmochim. Acta*, *43*, 1475–1498, 1979.

Swindle, T. D., M. W. Caffee, C. M. Hohenberg, G. B. Hudson, and R. S. Rajan, Noble gases in SNC meteorites, *Meteoritics*, *19*, 318–319, 1984.

Thomson, J. L., and J. W. Salisbury, The mid-infrared reflectance of mineral mixtures (7–14 μm), *Remote Sens. Environ.*, *45*, 1–13, 1993.

Treiman, A. H., and S. R. Sutton, Petrogenesis of the Zagami meteorite: Inferences from synchrotron X-ray (SXRF) microprobe and electron microprobe analyses of pyroxenes, *Geochim. Cosmochim. Acta*, *56*, 4059–4074, 1992.

Vincent, R. K., and G. R. Hunt, Infrared reflectance from mat surfaces, *Appl. Opt.*, *7*, 53–59, 1968.

Vincent, R. K., and F. Thomson, Spectral compositional imaging of silicate rocks, *J. Geophys. Res.*, *77*, 2465–2472, 1972.

Vincent, R. K., L. C. Rowan, R. E. Gillespie, and C. Knapp, Thermal-infrared spectra and chemical analyses of twenty-six igneous rock samples, *Remote Sens. Environ.*, *4*, 199–209, 1975.

Walter, L. S., and J. W. Salisbury, Spectral characterization of igneous rocks in the 8- to 12-μm region, *J. Geophys. Res.*, *94*, 9203–9213, 1989.

Wood, C. A., and L. D. Ashwal, SNC meteorites: Igneous rocks from Mars?, *Proc. Lunar Planet. Sci. Conf.*, *12th*, 1359–1375, 1981.

Wooden, J. L., C.-Y. Shih, I. E. Nyquist, B. M. Bansal, H. Wiesmann, and G. A. McKay, Rb-Sr and Sm-Nd isotopic constraints on the origin of EETA79001: A second Antarctic shergottite (abstract), *Lunar Planet. Sci.*, *13*, 879–880, 1982.

Yoder, H. S., and C. E. Tilley, Origin of basaltic magmas: An experimental study of natural and synthetic rock systems, *J. Petrol.*, *3*, 342–532, 1962.

P. R. Christensen and V. E. Hamilton, Department of Geology, Box 871404, Arizona State University, Tempe, AZ 85287-1404. (e-mail: hamilton@esther.la.asu.edu)

H. Y. McSween Jr., Department of Geological Sciences, University of Tennessee, Knoxville, TN 37916.

(Received December 2, 1996; revised June 23, 1997;
accepted June 27, 1997.)